CMI

www.nature.com/cmi

CORRESPONDENCE

Bypassing PELO-mediated ATPase activation of the NLR is a common pathogenic cause of *NLR*-associated autoinflammatory diseases

Xiurong Wu[1,2,6]✉, Zhang-Hua Yang[3,4,6], Yue Zheng[1], Jianfeng Wu[1,5] and Jiahuai Han[1,3,5]✉

Cellular & Molecular Immunology; https://doi.org/10.1038/s41423-024-01162-w

Nucleotide-binding and oligomerization domain (NOD)-like receptors (NLRs) are evolutionarily conserved intracellular pattern recognition receptors (PRRs) that sense microbial and danger signals, trigger immediate host defenses, and prime the adaptive immune response for long-lasting protection [1]. In humans, 22 known NLRs exist, and mutations in NLR family genes are associated with a wide range of inflammatory and autoimmune conditions, including hereditary periodic fever syndromes, Crohn's disease, Blau's syndrome, infantile enterocolitis, multiple sclerosis, and asthma [2, 3]. Collectively, these disorders can be categorized as *NLR*-associated autoinflammatory diseases.

The hallmark feature of NLRs is their central NOD (or NACHT) domain—an ATPase domain—while the N-terminal and C-terminal domains exhibit variability. Most NLRs have a C-terminal leucine-rich repeat (LRR). The N-terminal varies among NLRs and is responsible for homotypic protein-protein interactions [4]. The C-terminal LRR functions as an inhibitory domain in NLRs, and the NACHT domain hydrolyzes ATP upon activation. After ligand binding, the C-terminal LRR domain of most NLRs undergoes a conformational change, exposing the N-terminal domain. This conformational shift allows for the formation of oligomeric scaffolds, which subsequently interact with downstream signaling adaptors or effectors. Notably, ATPase activity within NLRs is essential for complex formation [4]. Despite the diversity of inflammatory pathways activated by different NLR family members, recent research has revealed a common checkpoint of ATPase activation that could govern the activation of all NLRs [5].

Protein pelota homolog (PELO) is a conserved component of the ribosome-associated quality control machinery. It functions as a surveillance factor in translational quality control and ribosome rescue [6–10]. Recently, we reported that PELO is essential for the activation of all the cytosolic NLR family proteins we tested. The underlying mechanism involves PELO recruitment by NLR proteins upon activation, catalyzing the activation of the ATPase within the NACHT domain of NLRs [5]. Because ATPase activity is essential for NLR activation, the effect(s) of pathogenic and nonpathogenic alterations on NLR ATPase activation mediated by PELO deserves investigation.

In our analysis, we focused on NLRP3, one of the most extensively studied NLR family members [11]. NLRP3 forms an inflammasome—an intracellular multimeric protein complex—in response to various exogenous microbial infections and endogenous danger signals [12]. Numerous mutations in NLRP3 have been reported, and these mutations are associated with autoinflammatory diseases such as cryopyrin-associated periodic syndrome (CAPS). Interestingly, CAPS can occur not only as a result of an inherited genetic mutation but also sporadically due to de novo or somatic mosaic NLRP3 mutations [13]. In our investigation, we initially analyzed the five most frequent gain-of-function germline mutants of NLRP3 to assess their impact on ATPase activation by PELO [13]. We expressed and purified NLRP3 and its mutants from *PELO* knockout HEK293T cells (Supplementary Fig. S1A) and measured their ATPase activity. Consistent with previous reports [5], the addition of purified recombinant PELO protein substantially increased the ATPase activity of NLRP3 (Fig. 1A). Interestingly, these five NLRP3 mutants exhibited high ATPase activity, and the addition of PELO had minimal or no effect on further enhancing their ATPase activity (Fig. 1A). Consequently, these disease-causing NLRP3 mutants can bypass the PELO-mediated activation step because they are capable of self-activation.

To investigate the linkage between PELO-mediated ATPase activation and disease-causing NLRP3 mutants, we expanded our analysis to include 47 naturally occurring NLRP3 mutations. This comprehensive set encompasses germline and somatic mosaic mutants, as well as pathogenic and nonpathogenic variants [13]. The ATPase activities of these strains with and without PELO activation are shown in Supplementary Fig. S1B. To show the relevant information collectively, we calculated the basal activity levels of each mutant relative to the full activation achieved through incubation with PELO based on the data in Supplementary Fig. S1B, which should represent the degree by which these mutants bypass PELO-mediated activation; we included the domain locations of each mutant and their disease-causing potential and showed all of this information in Fig. 1B. Our findings revealed a consistent pattern; pathogenic mutations within the

[1]State Key Laboratory of Cellular Stress Biology, School of Life Sciences, Faculty of Medicine and Life Sciences, Xiamen University, Xiamen, Fujian 361102, China. [2]Zhejiang Provincial Key Laboratory of Pancreatic Disease, MOE Joint International Research Laboratory of Pancreatic Diseases, The First Affiliated Hospital, Zhejiang University School of Medicine, Hangzhou 310012, China. [3]Research Unit of Cellular Stress of CAMS, Xiang'an Hospital of Xiamen University, Cancer Research Center of Xiamen University, School of Medicine, Faculty of Medicine and Life Sciences, Xiamen University, Xiamen, Fujian 361102, China. [4]Department of Gastroenterology, Sir Run Run Shaw Hospital, Zhejiang University School of Medicine, Hangzhou 310012, China. [5]Laboratory Animal Center, Xiamen University, Xiamen, Fujian 361102, China. [6]These authors contributed equally: Xiurong Wu, Zhang-Hua Yang. ✉email: xiurongwu@zju.edu.cn; jhan@xmu.edu.cn

Received: 10 March 2024 Accepted: 1 April 2024
Published online: 17 April 2024

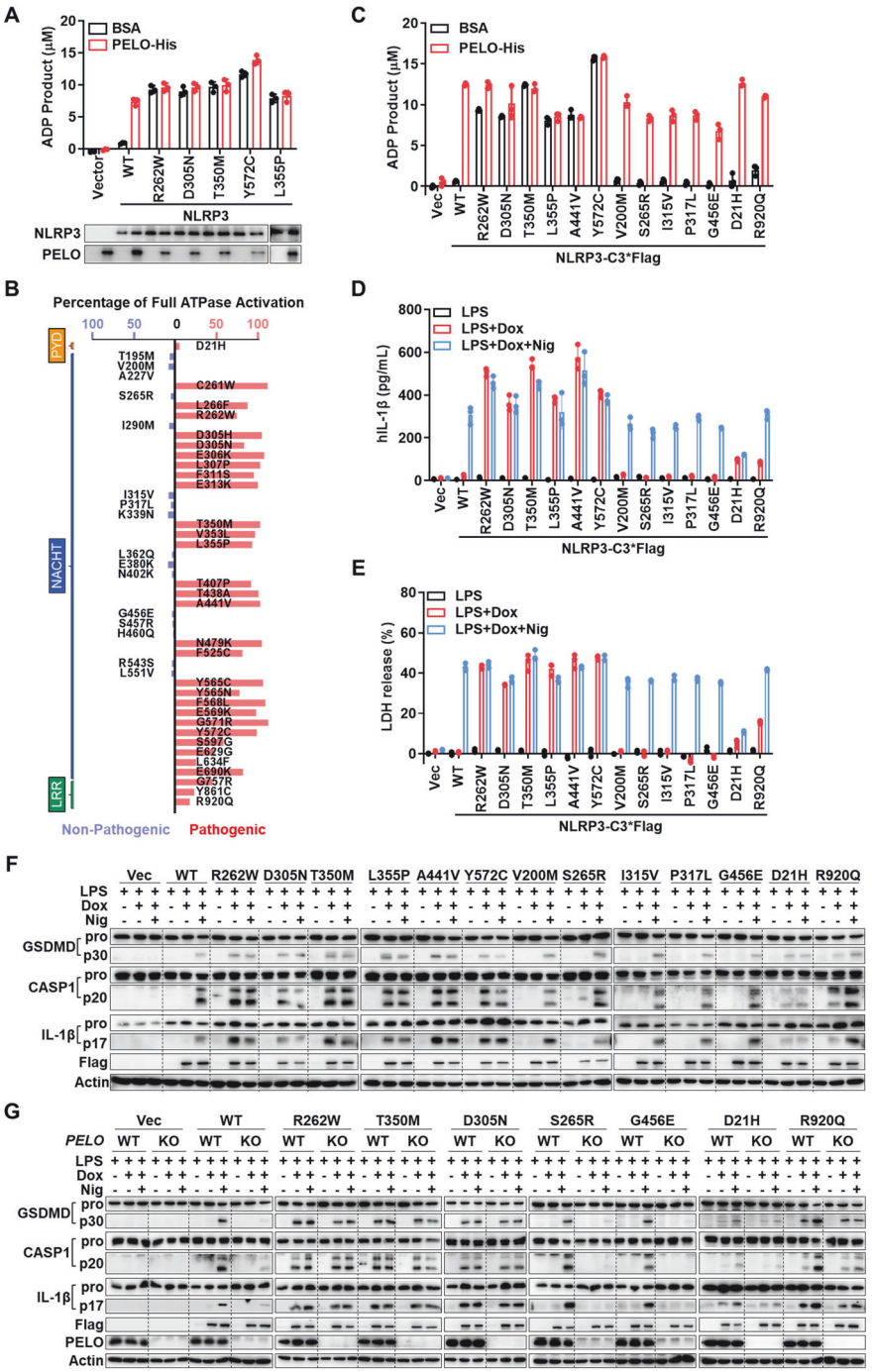

Fig. 1 Pathogenic NLRP3 mutations lead to the bypass of PELO-mediated ATPase activation of NLRP3 via an increase in ATPase activity, and each gain-of-function NLRP3 mutation spontaneously elicits inflammasome activation. A Purified Flag-WT or one of the five mutated NLRP3 proteins (100 ng) as indicated were incubated with BSA or recombinant PELO protein (50 ng) in the presence of 20 μM ATP, and the amount of the ADP product was measured using the ADP-Glo assay. **B** The experiments were performed as in **A** with 47 NLRP3 mutants. Schematics showing the basal ATPase activity of each NLRP3 mutant relative to the full activation induced by incubation with PELO. Pathogenic mutations are shown in red, and nonpathogenic mutations are shown in blue. The positions of the bars of each mutant in the schematic diagram correspond to the domain location of each mutation site. **C** ATPase activity of the 13 selected NLRP3 mutants. The data are derived from Supplementary Fig. S1B. **D**–**F** *NLRP3* KO THP-1 cells with stable integration of a Dox-inducible expression vector containing Flag-NLRP3 WT or one of the selected NLRP3 mutants were first primed with 1 mg/ml LPS for 4 hours. Following priming, the medium was replaced with medium supplemented with or without 1 μg/ml doxycycline (Dox). Six hours later, the cells were stimulated with or without 5 μM nigericin (Nig) for another hour. The supernatants were analyzed for IL-1β (**D**) and LDH (**E**); the pooled cell extracts and supernatants were analyzed by immunoblotting with anti-GSDMD, anti-caspase-1 (CASP1), anti-IL-1β and anti-actin (**F**) antibodies. **G** *NLRP3* KO THP-1 cells with and without additional *PELO* KO were stably transfected with a Dox-inducible expression vector of Flag-NLRP3 WT or one of the designated mutants and were treated with the stimuli described in **F**. The levels of processed GSDMD, caspase-1 (CASP1) and IL-1β in the pooled cell extracts and supernatants were analyzed by immunoblotting. Equal loading of the proteins in the ATPase activity assay was monitored by Western blotting (WB). The data are presented as the mean ± SD of triplicate samples (**A**, **C**, **D** and **E**). The rearranged noncontiguous WB lanes from the parallel processed gels are separated by a thin frame. All results are representative of at least two independent experiments

NACHT domain exhibited high basal ATPase activity, whereas nonpathogenic mutants exhibited no spontaneous activation (Fig. 1A, B and Supplementary Fig. S1B). Interestingly, mutations occurring outside the NACHT domain—such as those in the LRR domain—can also increase basal ATPase activity, which is further enhanced by PELO (Fig. 1B and Supplementary Fig. S1B). Remarkably, even though these LRR mutations only exhibit modest basal ATPase activity, they are pathogenic. Notably, the gain-of-function effects of the pathogenic NLRP3 mutants on PELO-mediated ATPase activation are not linked to any changes in their ability to interact with PELO (Supplementary Fig. S1C). Thus, the ability to bypass the PELO checkpoint and directly self-activate ATPase has emerged as a common feature among pathogenic NLRP3 mutants.

To investigate whether gain-of-function mutations in ATPase activate NLRP3, we analyzed inflammasome activation using an *NLRP3*-knockout human monocyte cell line (THP-1). The key features of inflammasome activation include caspase-1 activation, which initiates the maturation of the proinflammatory cytokines interleukin-1β (IL-1β) and/or IL-18, and cleavage of gasdermin D (GSDMD) to generate the N-terminal fragment, which induces pore formation, cytokine release, and pyroptosis [11]. Although NLRP3 and pro-IL-1β expression is typically induced by lipopolysaccharide (LPS) in standard cell models, our study employed *NLRP3* knockout THP-1 cells in which NLRP3 or its mutants were induced *via* a doxycycline (Dox)-inducible system. Thirteen mutants harboring both pathogenic and nonpathogenic mutations across distinct domains of NLRP3 were selected for evaluation. As already described in Supplementary Fig. S1B, the pathogenic mutants in these 13 mutants had spontaneous activity, while the nonpathogenic mutants required PELO for ATPase activation (Fig. 1C). In the standard experimental procedure, nigericin (Nig) was used to induce caspase-1 activation, IL-1β maturation and secretion, and pyroptosis in LPS-primed THP-1 cells. The experimental procedure was as follows: following LPS priming, the cells were stimulated with either nothing, Dox alone, or Dox in combination with Nig. IL-1β secretion was quantified by assessing IL-1β levels in the cell culture medium (Fig. 1D), while pyroptosis was evaluated through lactate dehydrogenase (LDH) release into the medium (Fig. 1E). Additionally, IL-1β maturation, caspase-1 cleavage, and GSDMD cleavage were determined by Western blotting (Fig. 1F). The results revealed an unresponsive phenotype in *NLRP3* knockout THP-1 cells to LPS, LPS+Dox, and LPS+Dox+Nig. Induction of NLRP3 expression by Dox restored the response to LPS+Nig to a level comparable to that in wild-type THP-1 cells. The induced expression of NLRP3 mutants with spontaneous ATPase activation directly triggers caspase-1 activation, GSDMD cleavage, and IL-1β maturation and secretion in the absence of secondary stimulation (nigericin). In contrast, mutants that do not exhibit gain-of-function ATPase activity do not directly activate the NLRP3 inflammasome; instead, they behave similarly to wild-type NLRP3 and respond to nigericin. Notably, the D21H mutant exhibits distinct behavior from other pathogenic mutants, likely due to its location in the PYD domain, which interacts with the downstream adaptor protein ASC [14]. Collectively, these data support the notion that ATPase activation by PELO serves as a checkpoint for NLRP3 inflammasome activation and that gain-of-function ATPase mutations bypass this checkpoint.

To confirm that PELO controls this checkpoint, we conducted the aforementioned experiments in cells with and without additional *PELO* deletion. As expected, *PELO* deficiency affected only wild-type NLRP3 and the mutants that did not exhibit basal ATPase activity (Fig. 1G). Conclusively, each gain-of-function ATPase mutation in NLRP3 bypassed PELO for ATPase activation, resulting in spontaneous inflammasome activation.

Next, we investigated whether the conclusions drawn from the study of NLRP3 could be extended to other NLR family members. NLRC4, another well-studied NLR, is associated with autoinflammatory diseases such as autoinflammation and infantile enterocolitis (AIFEC). Similar to our NLRP3 study, we selected specific NLRC4 mutants and assessed their ATPase activation by PELO in vitro (Supplementary Fig. S2A, B). The results mirrored those obtained for NLRP3: all mutants (highlighted in red) with pathogenic mutations in the NACHT domain bypassed the PELO checkpoint and gained basal ATPase activity. Conversely, PELO remained necessary for ATPase activation in mutants with nonpathogenic mutations (highlighted in blue) in the NACHT domain. In line with the NLRP3 findings, pathogenic mutations in the CARD domain showed no functional relationship with the PELO checkpoint for ATPase activation, while LRR domain mutations partially bypassed this checkpoint. Although mutations have been identified in most, if not all, NLR family members, disease-associated studies have primarily focused on NLRP3 and NLRC4 with some studies on NOD1, NOD2, NLRP7, and NLRP12. To further explore the impact of the PELO checkpoint on these additional NLRs, we examined the effect of PELO on the ATPase activity of these NLRs with pathogenic mutations in the NACHT domain. As depicted in Supplementary Fig. S2C–F, all of these mutations led to the bypass of PELO-mediated ATPase activation. Our data collectively demonstrate that bypassing the PELO checkpoint through gain-of-function ATPase mutations represents a common pathogenic mechanism in *NLR*-associated autoinflammatory diseases.

As the identification of sequence variations (including germline and somatic mutations) in NLRs continues to grow, assessing whether the PELO checkpoint for ATPase activation has been bypassed can serve as a valuable tool for classifying pathogenesis in patients with NLR mutations. Computational modeling of NLRP3 has been instrumental in evaluating the potential relationship between clinical severity and structural disruptions caused by mutations [15], but its feasibility is poor. By quantitatively determining both the extent of the bypass of the ATPase activation checkpoint by a mutation and whether PELO can further enhance ATPase activity in a given NLR mutant, we can explore the clinical implications. This includes assessing vulnerability to sterile or infectious inflammation and the potential for excessive immune reactions.

REFERENCES

1. Chen G, Shaw MH, Kim YG, Nunez G. NOD-like receptors: role in innate immunity and inflammatory disease. Annu Rev Pathol. 2009;4:365–98. https://doi.org/10.1146/annurev.pathol.4.110807.092239
2. Geddes K, Magalhaes JG, Girardin SE. Unleashing the therapeutic potential of NOD-like receptors. Nat Rev Drug Discov. 2009;8:465–79. https://doi.org/10.1038/nrd2783
3. Zhong Y, Kinio A, Saleh M. Functions of NOD-like receptors in human diseases. Front Immunol. 2013;4:333. https://doi.org/10.3389/fimmu.2013.00333
4. Meunier E, Broz P. Evolutionary convergence and divergence in NLR function and structure. Trends Immunol. 2017;38:744–57. https://doi.org/10.1016/j.it.2017.04.005
5. Wu X, Yang ZH, Wu J, Han J. Ribosome-rescuer PELO catalyzes the oligomeric assembly of NOD-like receptor family proteins via activating their ATPase enzymatic activity. Immunity. 2023;56:926–43.e927. https://doi.org/10.1016/j.immuni.2023.02.014.
6. Doma MK, Parker R. Endonucleolytic cleavage of eukaryotic mRNAs with stalls in translation elongation. Nature. 2006;440:561–4. https://doi.org/10.1038/nature04530
7. Shoemaker CJ, Eyler DE, Green R. Dom34:Hbs1 promotes subunit dissociation and peptidyl-tRNA drop-off to initiate no-go decay. Science. 2010;330:369–72. https://doi.org/10.1126/science.1192430
8. Pisareva VP, Skabkin MA, Hellen CU, Pestova TV, Pisarev AV. Dissociation by Pelota, Hbs1 and ABCE1 of mammalian vacant 80S ribosomes and stalled elongation complexes. EMBO J. 2011;30:1804–17. https://doi.org/10.1038/emboj.2011.93
9. Tsuboi T, Kuroha K, Kudo K, Makino S, Inoue E, Kashima I, et al. Dom34:hbs1 plays a general role in quality-control systems by dissociation of a stalled ribosome at the 3′ end of aberrant mRNA. Mol Cell. 2012;46:518–29. https://doi.org/10.1016/j.molcel.2012.03.013
10. Guydosh NR, Green R. Dom34 rescues ribosomes in 3′ untranslated regions. Cell. 2014;156:950–62. https://doi.org/10.1016/j.cell.2014.02.006
11. Broz P, Dixit VM. Inflammasomes: mechanism of assembly, regulation and signalling. Nat Rev Immunol. 2016;16:407–20. https://doi.org/10.1038/nri.2016.58
12. Guo H, Callaway JB, Ting JP. Inflammasomes: mechanism of action, role in disease, and therapeutics. Nat Med. 2015;21:677–87. https://doi.org/10.1038/nm.3893

13. Louvrier C, Assrawi E, El Khouri E, Melki I, Copin B, Bourrat E, et al. NLRP3-associated autoinflammatory diseases: Phenotypic and molecular characteristics of germline versus somatic mutations. J Allergy Clin Immunol. 2020;145:1254–61. https://doi.org/10.1016/j.jaci.2019.11.035
14. Hochheiser IV, Behrmann H, Hagelueken G, Rodríguez-Alcázar JF, Kopp A, Latz E, et al. Directionality of PYD filament growth determined by the transition of NLRP3 nucleation seeds to ASC elongation. Sci Adv. 2022;8:eabn7583. https://doi.org/10.1126/sciadv.abn7583
15. Samson JM, Ravindran Menon D, Vaddi PK, Kalani Williams N, Domenico J, Zhai Z, et al. Computational modeling of NLRP3 identifies enhanced ATP binding and multimerization in Cryopyrin-associated periodic syndromes. Front Immunol. 2020;11:584364. https://doi.org/10.3389/fimmu.2020.584364

ACKNOWLEDGEMENTS

We thank Lu Zhou for help with proofreading the manuscript. This work was supported by the National Natural Science Foundation of China (82388201 to JH, 32170751 to Z-HY), the Fundamental Research Funds for the Central Universities (226-2024-00015 to XW), the National Key R&D Program of China (2020YFA0803500 to JH), the CAMS Innovation Fund for Medical Science (2019-I2M-5-062 to JH), Fujian Province Central to Local Science and Technology Development Special Program (No. 2022L3079 to JH) and the Fu-Xia-Quan Zi-Chuang District Cooperation Program (No. 3502ZCQXT2022003 to JH).

AUTHOR CONTRIBUTIONS

XW and Z-HY performed most of the experiments; YZ and JW participated in the experiments; and XW, Z-HY, and JH analyzed the data and wrote the manuscript. XW and JH conceived the project and supervised the study.

COMPETING INTERESTS

The authors declare no competing interests.

ADDITIONAL INFORMATION

Supplementary information The online version contains supplementary material available at https://doi.org/10.1038/s41423-024-01162-w.

Correspondence and requests for materials should be addressed to Xiurong Wu or Jiahuai Han.

Supplementary Fig.1 Purified proteins and ATPase activity assay for NLRP3

(A) Representative image of silver staining of the purified proteins of Flag-tagged NLRP3 and its mutants as indicated.

(B) Purified Flag-WT or mutant NLRP3 proteins (100 ng) were incubated with BSA or recombinant PELO protein (50 ng) in the presence of 20 μM ATP, and the ADP product was measured using the ADP-Glo assay. Raw data of **Fig. 1B**.

(C) Flag-tagged WT or one of NLRP3 mutants as indicated was co-expressed with HA-tagged PELO in HEK293T cells. The cell lysates were immunoprecipitated with anti-Flag antibodies. The cell lysates and immunoprecipitates were analyzed by immunoblotting as indicated.

Equal loading of the proteins in ATPase activity assay was monitored by Western blotting. Data are represented as mean ± SD of triplicates.

The re-arranged noncontiguous WB lanes from the parallel processed gels are separated by a thin frame.

All results are representative of at least two independent experiments.

Supplementary Fig.2 Bypass of PELO-mediated ATPase activation is a common mechanism underlying the pathogenicity of disease-causing mutations of NLR family members

(A) Representative image of silver staining of the purified Flag-tagged proteins of NLRC4 and its mutants as indicated by an arrow.

(B) Purified proteins of Flag-WT NLRC4 or one of the selected NLRC4 mutants (100 ng) were incubated with BSA or recombinant PELO protein (50 ng) in the presence of 20 μM ATP, and ADP product was measured using the ADP-Glo assay. The pathogenic mutations were highlighted in red, and the non-pathogenic mutations were in blue.

(C-E) Representative image of silver staining of the purified Flag-tagged proteins as indicated by an arrow.

(F) Purified proteins of Flag-NLRP7, Flag-NLRP12, Flag-NOD1, Flag-NOD2 or their pathogenic mutations (100 ng) were incubated with BSA or recombinant PELO protein (50 ng) in the presence of 20 μM ATP, and ADP product was measured using the ADP-Glo assay.

Equal loading of the proteins in ATPase activity assay was monitored by Western blotting. Data are represented as mean ± SD of triplicates.

The re-arranged noncontiguous WB lanes from the parallel processed gels are separated by a thin frame.

All results are representative of at least two independent experiments.

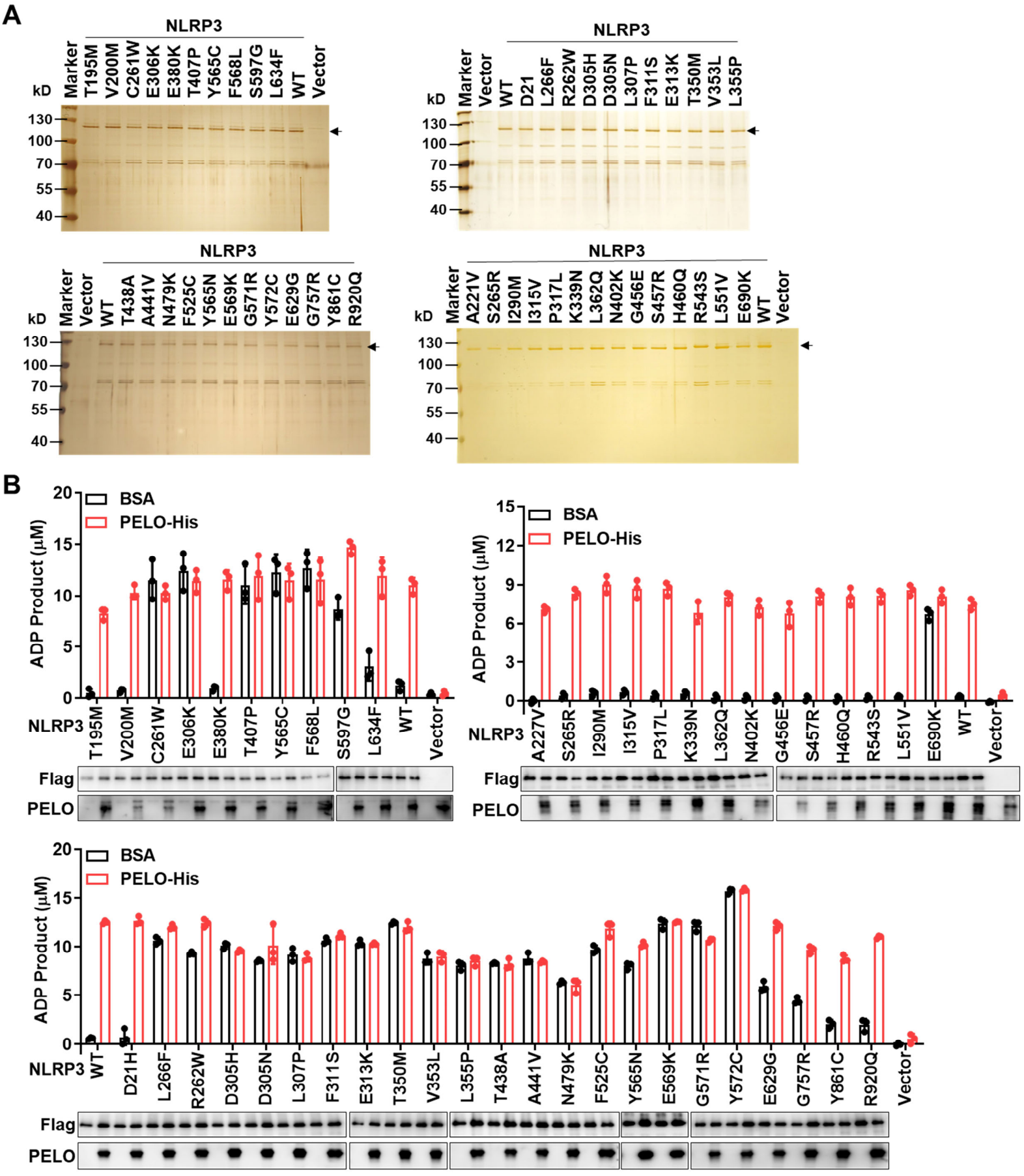
A
NLRP3
Marker
T195M
V200M
C261W
E306K
E380K
T407P
Y565C
F568L
S597G
L634F
WT
Vector
kD
130
100
70
55
40
NLRP3
Marker
Vector
WT
D21
L266F
R262W
D305H
D305N
L307P
F311S
E313K
T350M
V353L
L355P
NLRP3
Marker
Vector
WT
T438A
A441V
N479K
F525C
Y565N
E569K
G571R
Y572C
E629G
G757R
Y861C
R920Q
NLRP3
Marker
A221V
S265R
I290M
I315V
P317L
K339N
L362Q
N402K
G456E
S457R
H460Q
R543S
L551V
E690K
WT
Vector
B
BSA
PELO-His
ADP Product (μM)
NLRP3
T195M
V200M
C261W
E306K
E380K
T407P
Y565C
F568L
S597G
L634F
WT
Vector
Flag
PELO
BSA
PELO-His
ADP Product (μM)
NLRP3
A227V
S265R
I290M
I315V
P317L
K339N
L362Q
N402K
G456E
S457R
H460Q
R543S
L551V
E690K
WT
Vector
Flag
PELO
BSA
PELO-His
ADP Product (μM)
NLRP3
WT
D21H
L266F
R262W
D305H
D305N
L307P
F311S
E313K
T350M
V353L
L355P
T438A
A441V
N479K
F525C
Y565N
E569K
G571R
Y572C
E629G
G757R
Y861C
R920Q
Vector
Flag
PELO
C
Flag-NLRP3
WT
R262W
T350M
S265R
G456E
D21H
R920Q
Vector
HA-PELO + + + + + + + +
Input
Flag
PELO
IP: Flag
Flag
PELO

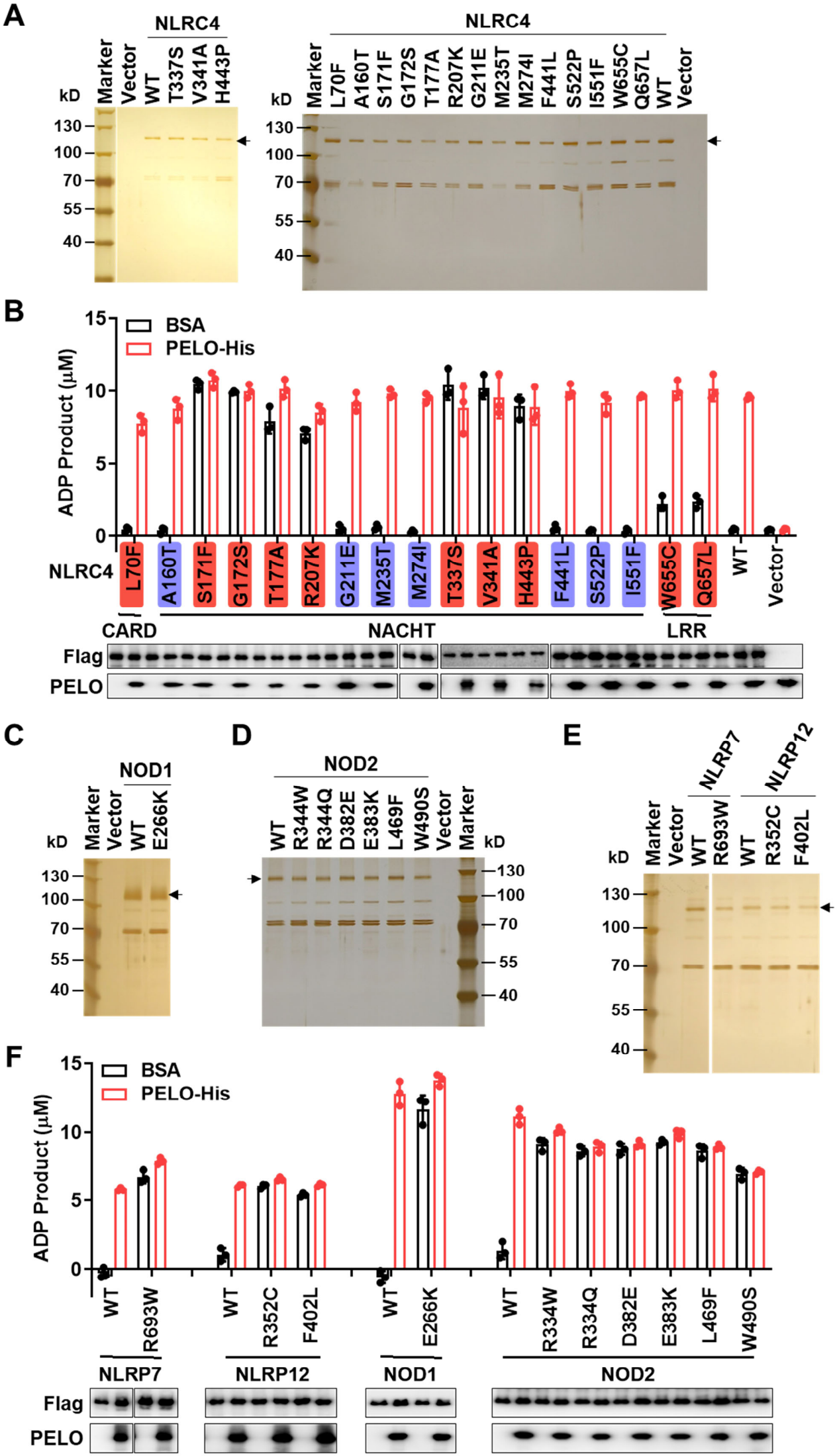
A
NLRC4
Marker
Vector
WT
T337S
V341A
H443P
kD
130
100
70
55
40
NLRC4
Marker
L70F
A160T
S171F
G172S
T177A
R207K
G211E
M235T
M274I
F441L
S522P
I551F
W655C
Q657L
WT
Vector
B
BSA
PELO-His
ADP Product (μM)
15
10
5
0
NLRC4
L70F
A160T
S171F
G172S
T177A
R207K
G211E
M235T
M274I
T337S
V341A
H443P
F441L
S522P
I551F
W655C
Q657L
WT
Vector
CARD
NACHT
LRR
Flag
PELO
C
NOD1
Marker
Vector
WT
E266K
kD
130
100
70
55
40
D
NOD2
WT
R344W
R344Q
D382E
E383K
L469F
W490S
Vector
Marker
kD
130
100
70
55
40
E
NLRP7
NLRP12
Marker
Vector
WT
R693W
WT
R352C
F402L
kD
130
100
70
55
40
F
BSA
PELO-His
ADP Product (μM)
15
10
5
0
WT
R693W
WT
R352C
F402L
WT
E266K
WT
R334W
R334Q
D382E
E383K
L469F
W490S
NLRP7
NLRP12
NOD1
NOD2
Flag
PELO

Materials and Methods:

Cell lines

The HEK293T cells were grown in DMEM supplemented with 10% FBS, and THP-1 cells were cultured in RPMI 1640 medium supplemented with 10% FBS. All cells were maintained at 37 °C in a 5% CO2 incubator.

Lentivirus production and infection

The lentiviral vectors, containing cDNAs or gRNAs of interest, were transfected into HEK293T cells along with lentivirus-packing plasmids (PMDL/REV/VSVG) using the calcium phosphate precipitation method. After 12 hours, the cell culture medium was changed and the virus-containing medium was collected 30 hours later. THP-1 cells were infected with lentiviral particles in the presence of 10 μg ml^{-1} polybrene and then centrifuged at 2,500 rpm for 60 min.

CRISPR-Cas9 knockout cells

The target sequences used were 5'-ATTGAAGTCGATCATTAGCG-3' for human *NLRP3* and 5'-GGCTTACCACACCATCGAGC-3' for human *PELO*. To construct the knockout cell lines, gRNA was transduced into THP-1 cells via lentiviral delivery, followed by blasticidin (10 μg ml^{-1}) selection. Single-cell clones were obtained through limiting dilution cloning in 96-well plates, and subsequently screened for the expression of the indicated genes using western blot. The selected knockout clones were further confirmed by DNA sequencing.

Stable cell lines

The Tet-On system was used for inducible expression of NLRP3 mutations in THP-1 cells. Initially, THP-1 cells were infected with lentivirus encoding the Tet-On 3G transactivator protein and subsequently subjected to selection using blasticidin (10 μg ml^{-1}). The resulting selected cells were utilized for subsequent experiments and further transduced with lentivirus carrying NLRP3 WT or mutations, followed by puromycin (10 μg ml^{-1}) selection.

Cell stimulation

THP-1 cells were initially primed with 1 mg ml^{-1} LPS for 4 hours in RPMI 1640 medium supplemented with 10% FBS. Following priming, the medium was replaced with serum-free RPMI 1640 medium containing 1 μg ml^{-1} doxycycline. Six hours later, the cells were stimulated with 5 μM nigericin for 1 hour. After stimulation, both culture supernatants and cell lysates were collected for immunoblotting analysis, with the cell supernatants were utilized for LDH assay (Cytotoxicity LDH Assay kit-WST, Dojindo Molecular Technologies) and ELISA analysis (human IL-1β ELISA Kit, Thermo Fisher Scientific) according to the manufacturer's instructions.

Recombinant protein preparation

As previously described[1], the C-terminal 6×His-tagged PELO protein was expressed in *E. coli* BL21 (DE3) strain (Novagen, Merck) by overnight culturing at 30 °C in an auto-induction medium. The PELO protein was purified with Ni^{2+}-NTA-agarose (Qiagen) and followed by further purification by Superdex 200 10/30 prepacked column (GE Healthcare). The protein concentration was determined using the BCA method with BSA as the standard.

NLR proteins preparation

The NLR proteins were purified as previously described[2]. Briefly, *PELO* KO HEK293T cells were transiently transfected with plasmids encoding 3×Flag-tagged NLRs. 36 hours after transfection, the cells were washed twice in cold PBS and lysed in lysis buffer (50 mM HEPES, pH7.4, 150 mM NaCl, 1% NP-40) supplemented with Protease Inhibitor Cocktail. The lysates were incubated at 4℃ on a rotation platform for 30 min and then centrifuged at 20, 000 g for 30 min at 4℃. The supernatants were pre-cleaned with IgG-Agarose at 4℃ on rotation for 2 hours, followed by incubation with Anti-Flag M2 Affinity Gel for 3 hours at 4℃ on rotation. The

beads were washed with wash buffer A (50 mM HEPES, pH7.4, 300 mM NaCl, 1% NP-40) for three times, followed by another three times of wash with wash buffer B (50 mM HEPES, pH7.4, 150 mM NaCl, 5% Glycerol, 10 mM $MgCl_2$, 0.1% NP-40). The NLR proteins were finally eluted with wash buffer B containing 200 μg ml^{-1} 3×Flag peptide.

ATPase activity assay

Assay was carried out using the ADP-Glo kinase assay kit in 384 Flat White Plates (142761, Thermo Fisher Scientific) as previously described[2]. Briefly, respective purified NLR proteins were incubated with BSA or PELO-His protein at 37°C for 30 min in the reaction buffer (50 mM HEPES, pH7.4, 150 mM NaCl, 5% Glycerol, 10 mM $MgCl_2$, 0.1% NP-40, 1 mM DTT). Further, a standard containing 20 μM ATP, 16 μM ATP and 4 μM ADP, 8 μM ATP and 12 μM ADP, or 20 μM ADP was prepared in the same buffer. After incubation, ATP (20 μM in final) was added to the mixture and further incubated at 37°C for another 60 min. The reaction is stopped by addition of ADP-Glo reagent and further incubated for 40 min at room temperature. After the addition of kinase detection buffer, samples were incubated for another 40 min and luminescence read out using a Spark 20M microplate reader (Tecan) with an integration time of 1 s per well. For calculation of the individual values, a linear regression was calculated based on the ADP standard.

Co-immunoprecipitation

HEK293T cells were lysed in NP-40 lysis buffer (25 mM HEPES, pH7.4, 150 mM NaCl, 1% NP-40) supplemented with Protease Inhibitor Cocktail. The lysates were incubated on a rocking platform for 30 min and then centrifuged at 20,000 g for 30 min at 4°C. Flag-tagged proteins were immunoprecipitated with Anti-Flag M2 Affinity Gel for 6 hours at 4°C. Beads containing protein complexes were washed with lysis buffer for three times. The immunocomplexes were eluted in SDS sample buffer and then analyzed by western blotting.

Statistical analysis

No statistical methods were used to predetermine sample size. GraphPad Prism software was used for data analysis. Data are shown as mean ± standard deviation (SD).

Resource availability

All data are available in the main text or the Supplementary Materials. All plasmids, reagents, cell lines and mouse lines generated in this study are available from the corresponding author.

KEY RESOURCES TABLE

REAGENT or RESOURCE	SOURCE	IDENTIFIER
Antibodies		
Rabbit anti-human IL-1β	Cell Signaling Technology	Cat# 12703S
Rabbit anti-human cleaved- IL-1β (Asp116)	Cell Signaling Technology	Cat# 83186S
Mouse anti-Caspase-1 (p20) (human)	AdipoGen	Cat# AG-20B-0048-C100
Rabbit anti-PELO	Abcam	Cat# ab309344
Rabbit anti-GSDMD	Novus Biologicals	Cat# NBP2-33422
Mouse anti DYKDDDDK-Tag (3B9)	Abmart	Cat# M20008M
Rabbit anti HA-Tag	Affinity	Cat# T0050
Mouse anti-Actin	Abmart	Cat# M20011
Chemicals, Peptides, and Recombinant Proteins		
LPS-EB Ultrapure	InvivoGen	Cat# tlrl-3pelps
Nigericin	InvivoGen	Cat# tlrl-nig
Blasticidin	Invitrogen	Cat# R210-01

Puromycin	Calbiochem	Cat# 540411
Doxycycline	MedChemExpress	Cat# HY-N0565B
Propidium iodide (PI)	Sigma	Cat# P4170
Polybrene	Sigma	Cat# H9268
Protease Inhibitor Cocktail	MedChemExpress	Cat# HY-K0010
Critical Commercial Assays		
Cytotoxicity LDH Assay kit-WST	Dojindo	Cat# CK12-2000
ADP-Glo™ Kinase Assay Kit	Promega	Cat# V6930
Human IL-1β ELISA Kit	Thermo Fisher Scientific	Cat# 88-7261-77
Fast Silver Stain Kit	Beyotime	Cat# P0017S
Toxin Eraser Endotoxin Removal Kit	GenScript	Cat# L00338
BCA Protein Assay Kit	Pierce	Cat# 23225
Experimental Models: Cell Lines		
Human: HEK293T	ATCC	Cat# CRL-3216
Human: THP-1	ATCC	Cat# TIB-202
Oligonucleotides		
sgRNA for human *PELO* KO cells: 5'-GGCTTACCACACCATCGAGC-3'	This paper	N/A
sgRNA for human *NLRP3* KO cells: 5'-ATTGAAGTCGATCATTAGCG-3'	This paper	N/A
Recombinant DNA		
pET28a-PELO	This paper	N/A
pBOBI-PELO	This paper	N/A
pBOBI-PELO-HA	This paper	N/A
pBOBI-NLRP3-3×Flag and its mutations	This paper	N/A
pBOBI-NLRC4-3×Flag and its mutations	This paper	N/A
pBOBI-NLRP7-3×Flag and its mutations	This paper	N/A
pBOBI-NLRP12-3×Flag and its mutations	This paper	N/A
pBOBI-NOD1-3×Flag and its mutations	This paper	N/A
pBOBI-NOD2-3×Flag and its mutations	This paper	N/A
pLVX-Tet3G	This paper	N/A
pLVX-TRE3G-NLRP3-3×Flag and its mutations	This paper	N/A
Other		
Ni-Sepharose resin	GE Healthcare	Cat# 17057502
Superdex G200 column	GE Healthcare	Cat# 17517501
Anti-Flag M2 Affinity Gel	Sigma	Cat# A2220

References

1 Wu, X. & Han, J. Protocol for reconstitution of oligomeric assembly of NAIP5-NLRC4 inflammasome in vitro. *STAR Protoc* 4, 102581, doi:10.1016/j.xpro.2023.102581 (2023).

2 Wu, X., Yang, Z. H., Wu, J. & Han, J. Ribosome-rescuer PELO catalyzes the oligomeric assembly of NOD-like receptor family proteins via activating their ATPase enzymatic activity. *Immunity* 56, 926-943 e927, doi:10.1016/j.immuni.2023.02.014 (2023).

Fig. 1A

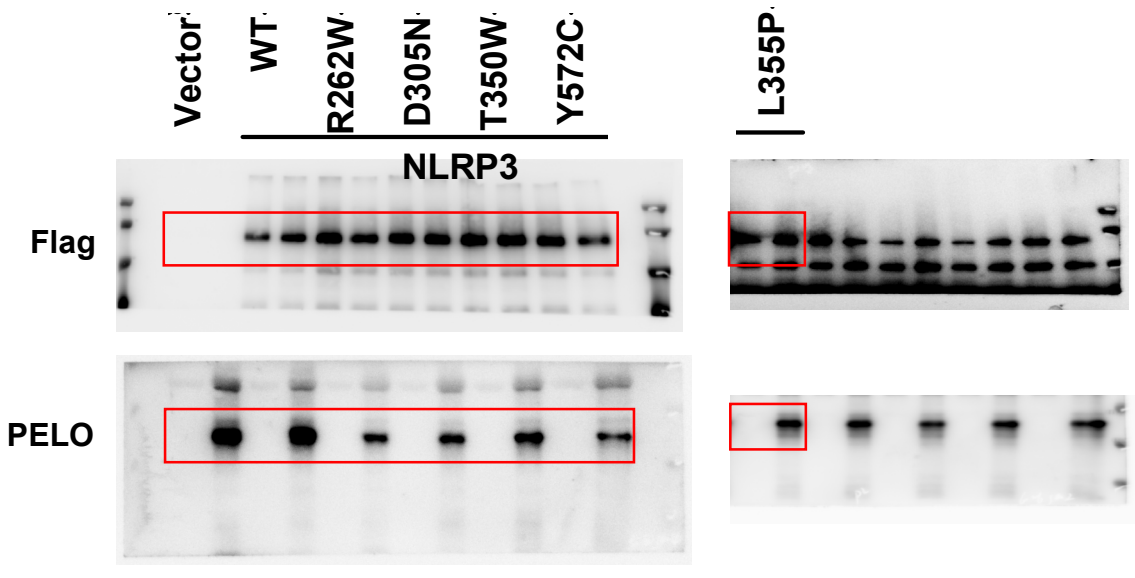

Fig. 1F

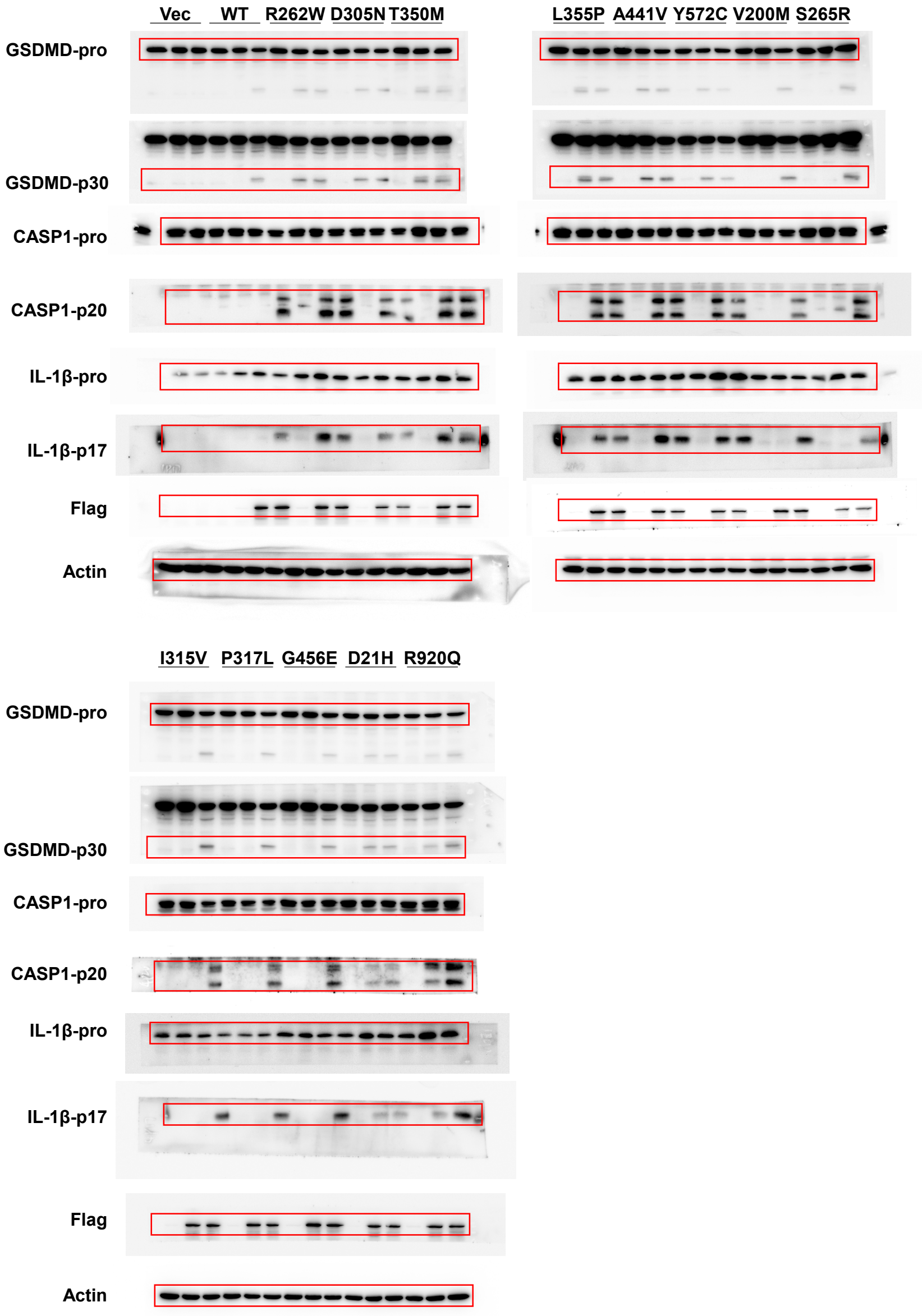
Vec
WT
R262W
D305N
T350M
L355P
A441V
Y572C
V200M
S265R
GSDMD-pro
GSDMD-p30
CASP1-pro
CASP1-p20
IL-1β-pro
IL-1β-p17
Flag
Actin
I315V
P317L
G456E
D21H
R920Q
GSDMD-pro
GSDMD-p30
CASP1-pro
CASP1-p20
IL-1β-pro
IL-1β-p17
Flag
Actin

Fig. 1G

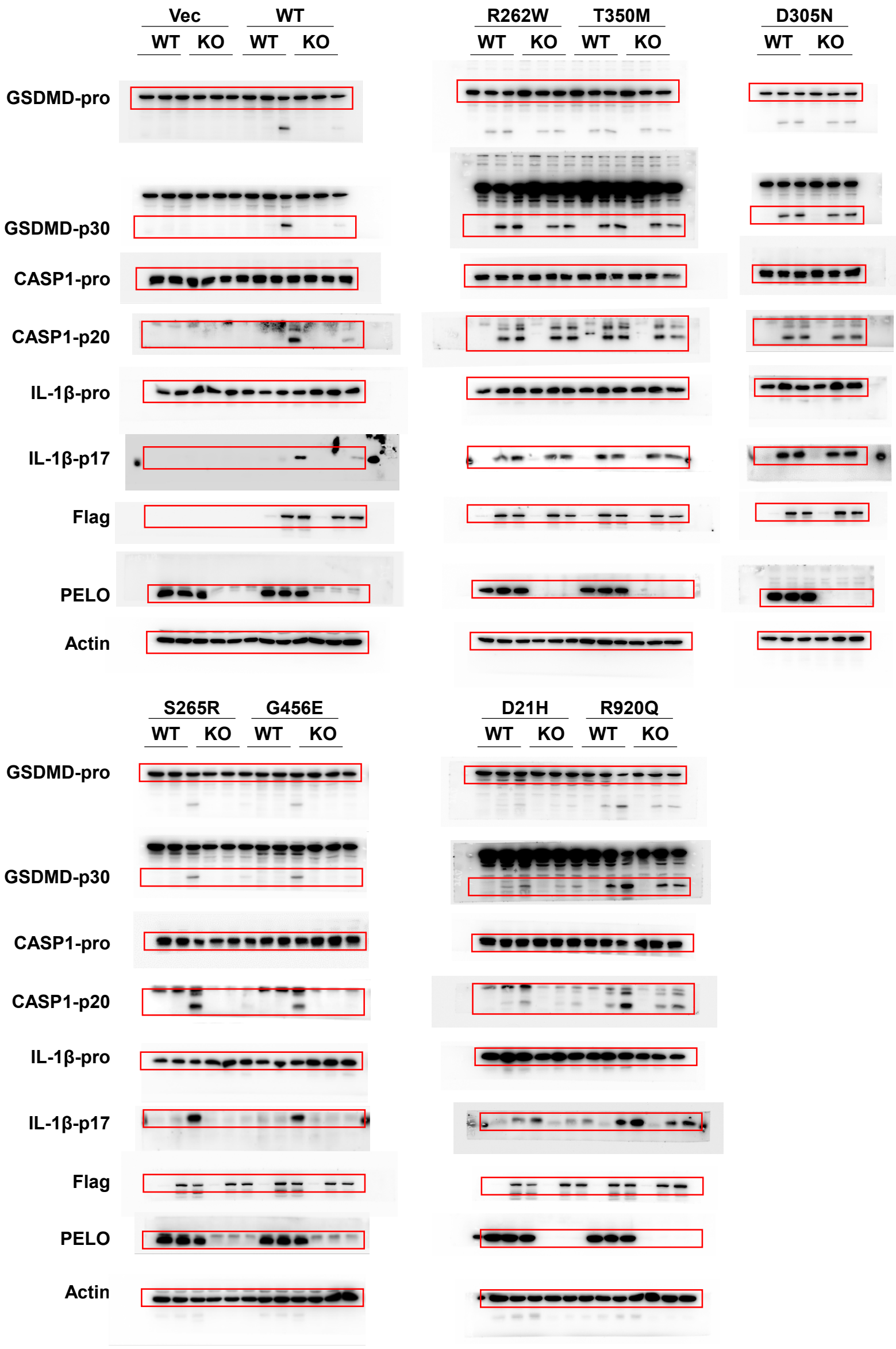
Vec
WT
KO
WT
KO
WT
KO
R262W
WT
KO
T350M
WT
KO
D305N
WT
KO
GSDMD-pro
GSDMD-p30
CASP1-pro
CASP1-p20
IL-1β-pro
IL-1β-p17
Flag
PELO
Actin
S265R
G456E
D21H
R920Q

Fig. S1B

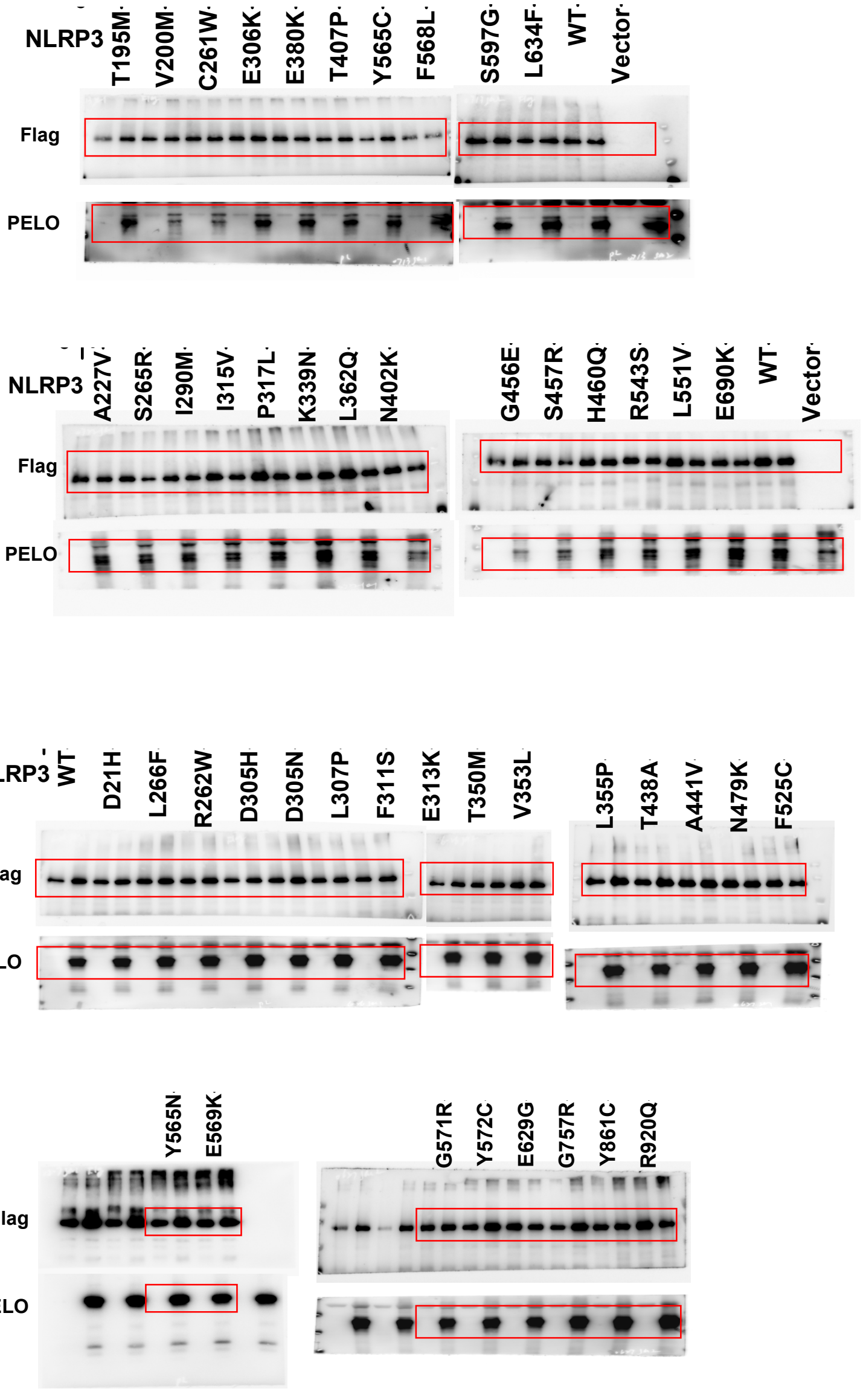
NLRP3
T195M
V200M
C261W
E306K
E380K
T407P
Y565C
F568L
S597G
L634F
WT
Vector
Flag
PELO
NLRP3
A227V
S265R
I290M
I315V
P317L
K339N
L362Q
N402K
G456E
S457R
H460Q
R543S
L551V
E690K
WT
Vector
Flag
PELO
NLRP3
WT
D21H
L266F
R262W
D305H
D305N
L307P
F311S
E313K
T350M
V353L
L355P
T438A
A441V
N479K
F525C
Flag
PELO
Y565N
E569K
G571R
Y572C
E629G
G757R
Y861C
R920Q
Flag
PELO

Fig. S1C

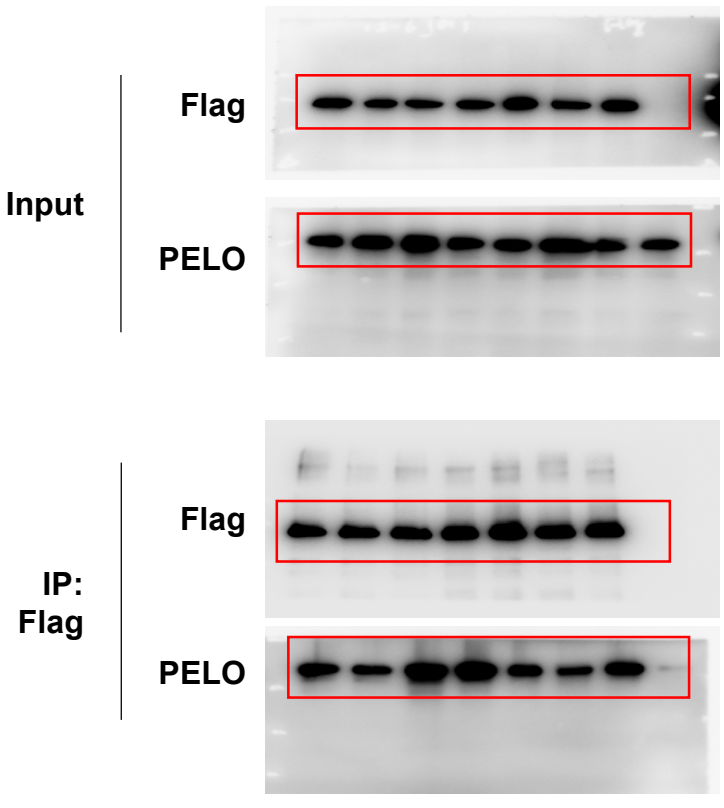

Fig. S2B

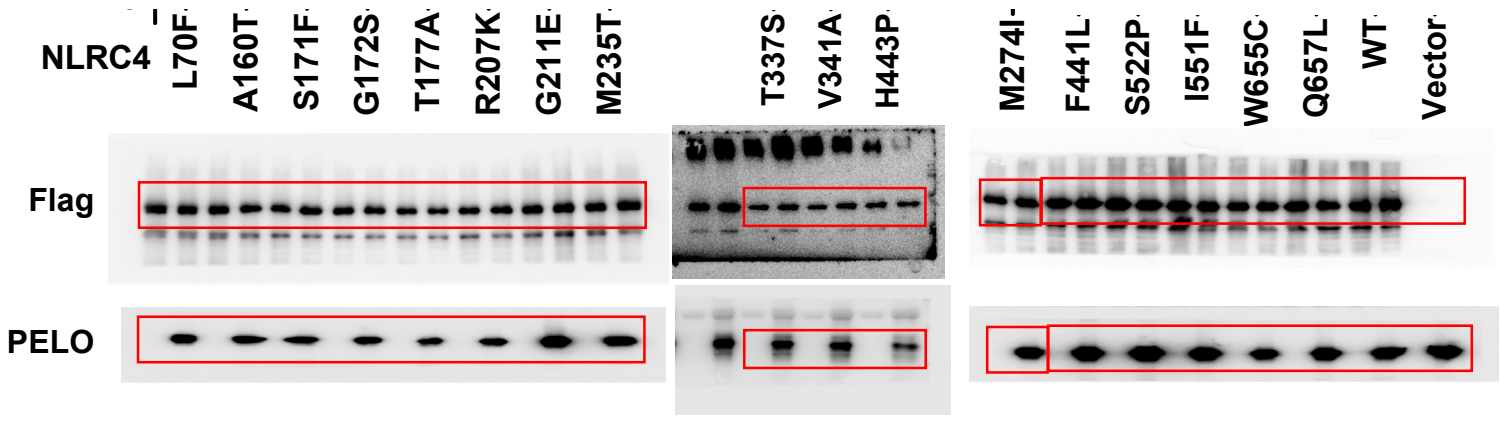
NLRC4
–
L70F
A160T
S171F
G172S
T177A
R207K
G211E
M235T
T337S
V341A
H443P
M274I
F441L
S522P
I551F
W655C
Q657L
WT
Vector
Flag
PELO

Fig. S2F

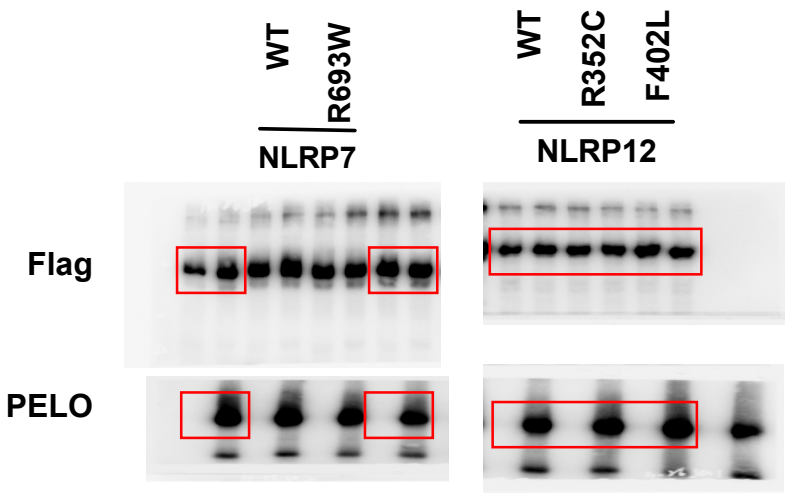
WT
R693W
NLRP7
WT
R352C
F402L
NLRP12
Flag
PELO

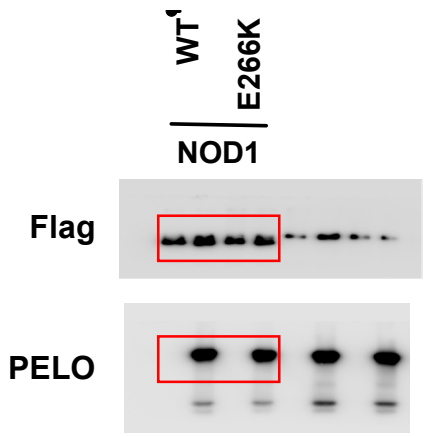
WT
E266K
NOD1
Flag
PELO

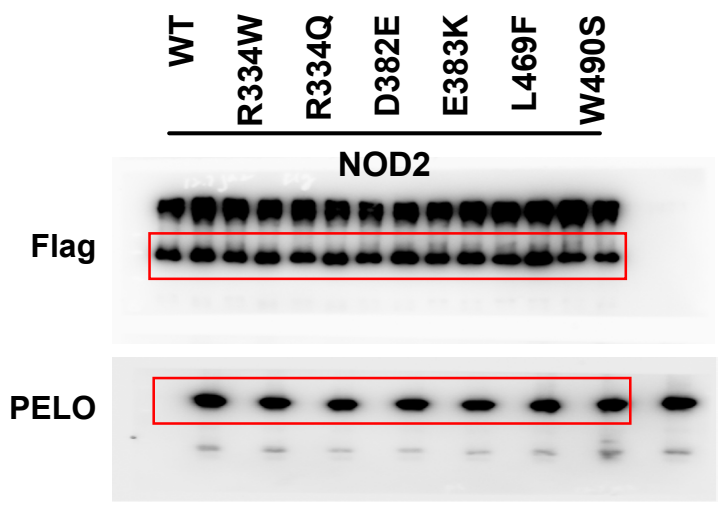
WT
R334W
R334Q
D382E
E383K
L469F
W490S
NOD2
Flag
PELO